Scientific Research Publishing

Atmospheric and Climate Sciences, 2023, 13, 431-454
https://www.scirp.org/journal/acs
ISSN Online: 2160-0422
ISSN Print: 2160-0414

Northeastern Tropical Atlantic SST and Sahel Rainfall Variability

Dahirou Wane*, Abdou Lahat Dieng, Coumba Niang, Amadou T. Gaye

Laboratoire de Physique de l'Atmosphère et de l'Océan Siméon Fongang, Ecole Supérieure Polytechnique, Université Cheikh Anta Diop de Dakar (LPAO-SF/ESP/UCAD), Dakar, Senegal
Email: *wane.dahirou@esp.sn, *mahasimw@gmail.com, atgaye@ucad.edu.sn

How to cite this paper: Wane, D., Dieng, A.L., Niang, C. and Gaye, A.T. (2023) Northeastern Tropical Atlantic SST and Sahel Rainfall Variability. *Atmospheric and Climate Sciences*, **13**, 431-454.
https://doi.org/10.4236/acs.2023.134024

Received: May 25, 2023
Accepted: August 28, 2023
Published: August 31, 2023

Abstract

The SST variability during the summer period in the northeastern tropical Atlantic region (NTA) is characterized by an alternation of warming/cooling which represents 87% of the total variability. The aim of this paper is to study the atmospheric responses as well as the precipitation associated with these oceanic conditions. Based on Reynolds's SST from 1982 to 2019, a normalized Northern Tropical Atlantic index (NTAI) is computed into the region between 15˚ - 25˚W; 12˚ - 16˚N and a composite analysis is then performed. It is shown that the NTAI is significantly correlated with the SST's first principal component mode (PC1) in this region. Moreover, the composite of SST anomalies and atmospheric parameters exhibits a strong local ocean-atmosphere interaction which highly impacts the large-scale atmospheric circulation in West Africa, particularly in the western Sahel. An in-depth analysis shows that the atmospheric response to the warm (cold) SST is a cyclonic (anticyclonic) circulation in the lower layers near the West Africa Coast. This cyclonic (anticyclonic) circulation strengthens/reduces the moisture transport towards the continent in the low levels. In the middle layers of the atmosphere (500 hPa), the warm (cold) composite is associated with a decrease (increase) in the intensity of the African Easterly Jet (AEJ) whereas, in the upper atmosphere (200 hPa), the strengthening (weakening) of the Tropical Easterly Jet (TEJ) is observed. With regard to the composite precipitation field, a positive/negative SST anomaly is associated with significantly enhanced/reduced rainfall in the western Sahelian region. It is found that this relationship (correlation) increases as we are closer to the coasts.

Keywords

SST-Rain, Sahel Rainfall, Senegal Rainfall, Ocean-Atmosphere Interaction

1. Introduction

The northeastern tropical Atlantic (NTA) is dominated by a pronounced seasonal and interannual cycle in Sea Surface Temperature (SST) and surface wind. Figure 1(a) shows the first empirical orthogonal function (EOF) mode of Reynolds monthly SST anomalies during June-September from 1982 to 2019. This figure shows that the interannual SST variation in the NTA region is characterized by the positive (negative) SST anomalies (SSTA) off the Senegalese coast. More closely connected with the seasonal cycle, NTA warming usually develops in boreal spring (March-May, MAM), peaks in the summer (June-August, JJA), and dissipates in autumn (September-November, SON). The warmest SST is observed in boreal summer when the Intertropical Convergence Zone (ITCZ) migrates northward. This migration leads to a slowdown of the northerly trade winds which induces a low-level wind convergence in the NTA region. Then, the SST gradually warms from April to September with a maximum located off the Senegalese-Mauritanian coast. Then, this SSTA variability confined off Senegal is explored from a new viewpoint of the ocean-land-atmosphere interaction [1]. The interannual variability of the regional mixed-layer temperature anomaly that evolves in boreal early summer and peaks in July-August is associated with the northern wind anomaly, mixed-layer depth anomaly, and atmospheric pressure gradient anomaly, suggesting the existence of ocean-land-atmosphere coupled processes. The NTA warming (cooling)'s oceanic aspect may be explained by the anomalously thin (thick) mixed layer, which absorbs shortwave surface heat flux.

The development of the northeastern tropical Atlantic SST anomalies is also attributed to remote atmospheric and oceanic forcing from the Pacific Ocean ([2] [3] [4]) or local air-sea interactions in the tropical northeastern Atlantic Ocean ([1] [5] [6]). The evolution of this coupled mode is locked to a boreal spring and develops through thermodynamic air-sea interaction linked with the ITCZ migration. Then, the weaker trade winds in the northern hemisphere associated with the anomalously northward shift of the ITCZ are responsible for warming SST anomalies thereby suppressing evaporation and thus latent heat loss. However, the acceleration of surface winds leads to an increase in evaporative heat loss and induces a cold SST anomaly. This process is known as the wind-evaporation-SST (WES) positive feedback ([7] [8]). [9] suggested that the SST variability would be a passive response of the ocean to seasonal winds, the latter being themselves a passive response to seasonal temperature changes in the West African continent. On the other hand, the SST influences the winds through thermodynamic or dynamic feedback, local or remote ([7] [10]). Although the north tropical Atlantic SST anomalies are significantly correlated with El Niño-Southern Oscillation (ENSO), the Indian Ocean Dipole (IOD) and the Interdecadal Pacific Oscillation ([3] [11] [12]). Recent studies have demonstrated that the coastal Niño/Niña events independently exert a substantial influence on the regional climate and marine ecosystems along the neighborhood regions ([13] [14]).

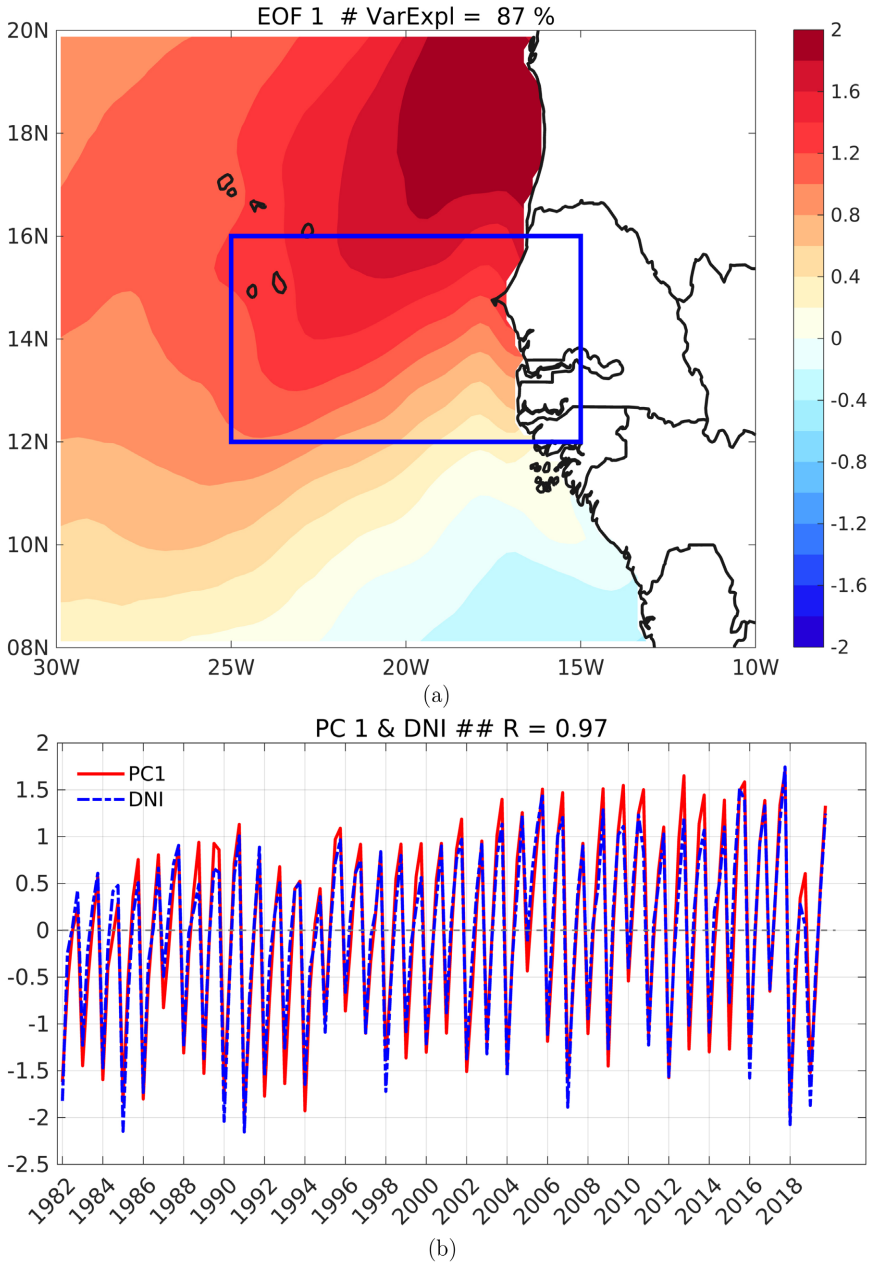

Figure 1. The spatiotemporal characteristics of northeastern tropical Atlantic. (a) First empirical orthogonal function (EOF) mode of monthly SST anomalies (˚C) during June-September 1982-2019 derived from TMI Reynolds data. The blue box in (a) denotes the region for the Northeastern Tropical Atlantic Index (NTAI). The percentage of total variance explained by the EOF1 reaches 87%. (b) Normalized time series of EOF1 (PC1, red solid curve) and NTAI (blue dashed curve) average for the region (25˚ - 15˚W, 12˚ - 16˚N) marked by the blue box in (a).

In many respects, the influence of the SST on West African rainfall variability has long been studied and a large number of papers ([15]-[21]) have investigated the influence of the tropical eastern Atlantic SST on West African rainfall. On a seasonal scale, West African rainfall is strongly conditioned by the evolution of the ITCZ ([15] [22]) which is influenced mainly by seasonal SST anomalies. [16]

showed a significant influence of the seasonal cooling of the Atlantic Cold Tongue (ACT) SST on the West African monsoon (WAM), through the intensification of the southerly winds in the ACT region and pushing the rain band north of the Guinean regions. Thus they show that the WAM remains blocked in the south if the cold tongue does not develop. Supporting this, other modelings ([19]) and diagnostic ([23]) studies found meridional SST and SLP gradients and meridional winds over the Gulf of Guinea to be tightly related, and these mechanisms strongly impact moisture flux convergence near the coast, leading to the installation of the first rainy season of the WAM system. This is confirmed by [17] and [21] who show a strong influence of the SST seasonal variations on the seasonal ITCZ and WAM variations, using an atmospheric general circulation model (AGCM). Indeed, SST Warming in this region leads to a southward migration of the ITCZ in the boreal summer of the ITCZ. To explain the mechanism of this influence, [24] suggests that the SST anomaly in the ACT contributes to the northward migration of moisture and convection and is associated with a possible jump in the West African monsoon.

In contrast to the southeastern region of the tropical Atlantic, the impact of the northeastern tropical Atlantic SST anomalies on the West African rainfall variability is poorly documented despite the important role of the West African Westerly Jet (WAWJ) on the Sahelian rainfall [25]. The atmospheric circulation in the lower layer is characterized by a northward flow over the ACT region and a southwesterly flow over West Africa which wraps around the thermal low over the central-east Sahara [26]. In the north tropical Atlantic, previous studies ([25] [26] [27]) show the existence of a relatively strong westerly flow with a maximum zonal component around 10˚N (8˚ - 11˚N) and speeds above 5 - 6 $m{\cdot}s^{-1}$ to the east of 20˚W: this jet is identified as the West African westerly jet. This jet is associated with a westward extension of the low thermal over the eastern Atlantic to about 35˚W [28]. It is clearly distinguished from the monsoon westerly flow by its structure and dynamics and plays an important role in transporting moisture from the tropical eastern Atlantic to Sahelian West Africa during boreal summer. [26] show that the variations of the WAWJ are significantly and positively correlated with precipitation variations over the Sahel on both interannual and decadal time scales. In wet (dry) periods over the Sahel, enhanced (decreased) westerly moisture fluxes are associated with a strong (weak) jet increase (decrease) the low-level moisture content over the Sahel, decreasing (enhancing) the stability of the atmosphere.

This paper focuses only on the effect of the northeastern Atlantic SST anomalies on West African rainfall, particularly over the Sahel. This study contributes to the understanding of the influence of SST anomalies on Sahelian rainfall which lead to an improvement in seasonal rainfall forecasts in this region. The article is organized as follows. Firstly we briefly introduce the data sets and methods used in this study. Then, we analyze the precipitation and large-scale atmospheric circulation anomalies associated with the NTA warming/cooling. Finally, the conclusion is presented in the summary section.

2. Data and Methodology

2.1. Data

The atmospheric reanalysis data, including three-dimensional winds, relative and specific humidity, divergence, and air temperature, were obtained from the European Center for Medium-Range Weather Forecasts (ECMWF) ERA5 reanalysis data set [29]. These data are available at a horizontal resolution of 0.25˚ × 0.25˚ and extend from 1000 to 100 hPa with 27 vertical pressure levels. The ERA5 data cover the study period from 1982 to 2019. The monthly data are used to provide monthly averaged atmospheric fields including horizontal wind, surface pressure, etc. The observed sea surface temperature (SST) fields are based on the National Oceanic and Atmospheric Administration (NOAA) Optimal Interpolated Sea Surface Temperature (OISST, [30]) data set, which provides global, gridded, daily-mean fields starting from 1982 with a horizontal resolution of 0.25˚ × 0.25˚. Version 4.04 of the Climatic Research Unit gridded Time Series (CRU-TS4.04, [31]) product is also adapted to provide the monthly averaged surface precipitation rate over West Africa. The rain rate data have a horizontal resolution of 0.5˚ × 0.5˚ and cover the study period from 1982 to 2019.

2.2. Methodology

2.2.1. Definition of the Northeastern Tropical Atlantic Warm Event

A conventional northeastern tropical Atlantic (NTA) warm event starts in June, matures in boreal summer (July-September), and finally decays in October [1]. Empirical orthogonal function (EOF) analysis has been frequently used to examine the temporal and spatial characteristics of NTA warm events ([13] [14]). To identify NTA warm events, an EOF analysis is performed on the monthly SSTAs from June to September 1982-2019 over the 30˚W - 10˚E, 8˚ - 20˚N domain. The first EOF (EOF1), which explains 87.4% of the total variance), captures the NTA warm SST pattern with the warmer-than-normal SST located off the West Africa coast (**Figure 1(a)**). The second EOF mode accounts for only 4.3% of the total variance (not shown). The normalized time series of the first principal component (PC1) well resembles the remarkable variability of the NTA index (NTAI) calculated by the averaged SSTA in the region of 25˚W-coast, 12˚ - 16˚N (see the blue box in **Figure 1(a)**), with simultaneous correlation coefficients of +0.97 (**Figure 1(b)**). Therefore, PC1 effectively provides a benchmark to denote the interannual variation in the NTA warm events.

2.2.2. Composite Method

For this work, a composite method is used to identify warm and cold summer seasons. The composite analysis is a very useful statistical tool to isolate the characteristics of a large number of cases of a given meteorological phenomenon over time and space in relation to a region of interest. It has clear advantages for extracting signals or interactions from a complex environment and allows in addition to observe whether a signal previously defined in a reference variable is found in other variables. The composite analyses were carried out using a cha-

racteristic index of SST anomalies in the NTA, called NTAI. This NTAI is constructed over the season from June-September for the period 1982-2019.

For this work, warm and cold years in the NTA region are defined using two thresholds: S_1 and S_2 in which $S_1 = 0.5 \times \sigma_{NTAI}$ and $S_2 = -0.5 \times \sigma_{NTAI}$. We defined warm years when the NTAI of a particular year is greater than S_1, cold years when the NTAI is less than S_2 and normal ones when the index is ranging between S_1 and S_2 (Figure 2). However, we did not consider the normal year for the purpose of this work. Thus, all years that are categorized as warm (cold) are classified as warm (cold) composite. The two indices associated with warm and cold years are averaged. Both averaged fields are then associated with the positive and negative SST anomalies phases and the difference between these two average fields is used to evaluate the amplitude of the average modulation. The advantage of this method is that there is no assumption made on the nature of the relationship (linear or not) between variables but rather on thresholds. In summary, a composite is defined as the average of the warmest or coldest years over the period considered.

2.2.3. Precipitable Water Vapor and Humidity Transport

Precipitable water vapor refers to the integrated water vapor content of an atmospheric column (Precipitable Water Vapor, PWV) and is defined as:

$$\mathrm{PWV} = \frac{1}{g}\int_{P_s}^{P_t} q\mathrm{d}p \tag{1}$$

where the moisture transport is analyzed using the approach of [32] [33] and [34]. The horizontal moisture flux vector, vertically integrated for different atmospheric layers, is given by (Equation (2)):

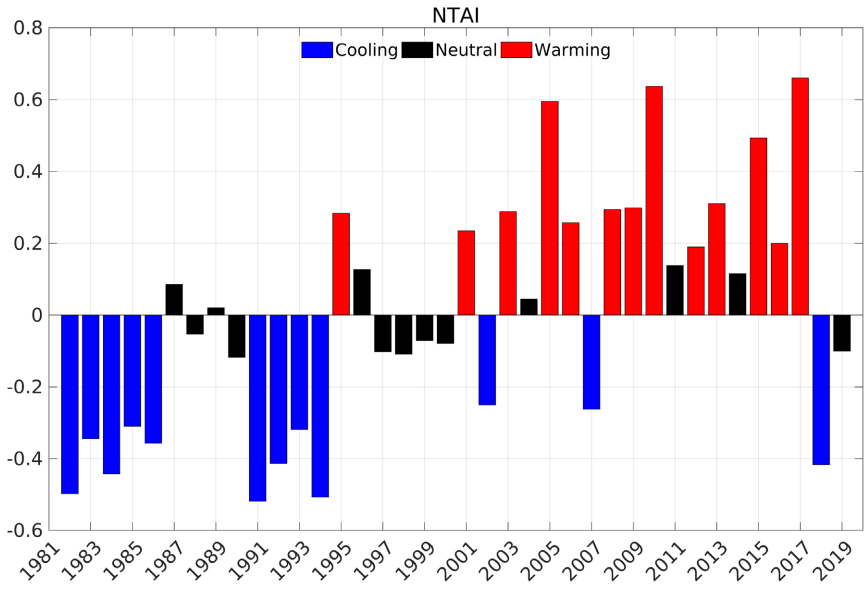

Figure 2. Normalized Northeastern Tropical Atlantic Index (ATNI) from 1982 to 2019. The cooling (warming) periods in this region are shown by the blue (red) bars showing the indices below (above) the standard deviation and, the black bars show the neutral periods.

$$Q = \frac{1}{T}\int_0^T -\frac{1}{g}\left(\int_{P_b}^{P_t} qV_h \mathrm{d}p\right)\mathrm{d}t \quad (2)$$

where g is the gravitational acceleration (9.8 $m{\cdot}s^{-2}$), q the specific humidity, V_h the horizontal wind, P_b and P_t the lower and upper limits of the vertical integration and T the temporal mean considered. In this study vertical integration is considered in three atmospheric layers: the low layer (from surface pressure, P_{surf}, to 850 hPa), the middle layer (700 - 500 hPa), and the upper layer (400 - 100 hPa). The cold and warm composites of these flows are shown in **Figure 5**.

3. Results and Discussion

3.1. Precipitation Anomalies Associated with the NTA SST Anomalies

Figure 3 shows the linear regression of PC1/NTAI onto June-September mean surface pressure (shaded), wind (vector), and SST anomalies (**Figure 3(a)**) and, precipitation (**Figure 3(b)**).

The regression map NTAI on the SSTA field (**Figure 3(a)** contour) shows a slightly different signal from that of the EOF1 mode however both highlight the maximum SSTA appearing along the West Africa coast with a warm tongue extending southwestward (**Figure 3(a)**). The NTA warm anomalies induce a reduction of surface pressure over the NTA region, generating a dipole with a region of low and high surface pressure located over the Ocean and Continent, respectively. This pattern of surface pressure is associated with a northward circulation which favors a northward humidity transport. This coupled feedback mechanism is often referred to as the Bjerknes feedback and has been shown to be an important component of equatorial Pacific and Atlantic variability ([35] [36] [37]). Surface wind is generally considered to be the result of a balance between pressure gradient force, Coriolis, and friction forces, generally neglecting the term advection as in the simple model of [38]. SST influences wind via a local modification of the pressure gradient ([39] mechanisms), opposing the large-scale pressure gradient, controlled by the free troposphere above the marine atmospheric mixing layer. In addition, variation in SST can influence surface winds through the mechanisms of [40] and [41] and stratification in the marine atmospheric boundary layer (MABL) by partially controlling the vertical flux of horizontal momentum. An anomaly in atmospheric circulation above the top of the MABL, where vertical gradients (moisture gradient) are very strong [34], could have a significant impact on surface winds.

In particular, significant positive precipitation anomalies are mainly observed off the coastal regions of WA (West of 10˚W) with counterpart a reduction of precipitation (**Figure 3(b)**) over the Guinean coastal region (South of 8˚N). The influence of the NTAI index on West African rainfall is more pronounced in the west and decreases considerably towards the eastern regions, particularly in the Sahelian region. This is in adequation with the enhanced rainfall signal over the Sahelian obtained by averaging the regression coefficients over the same region

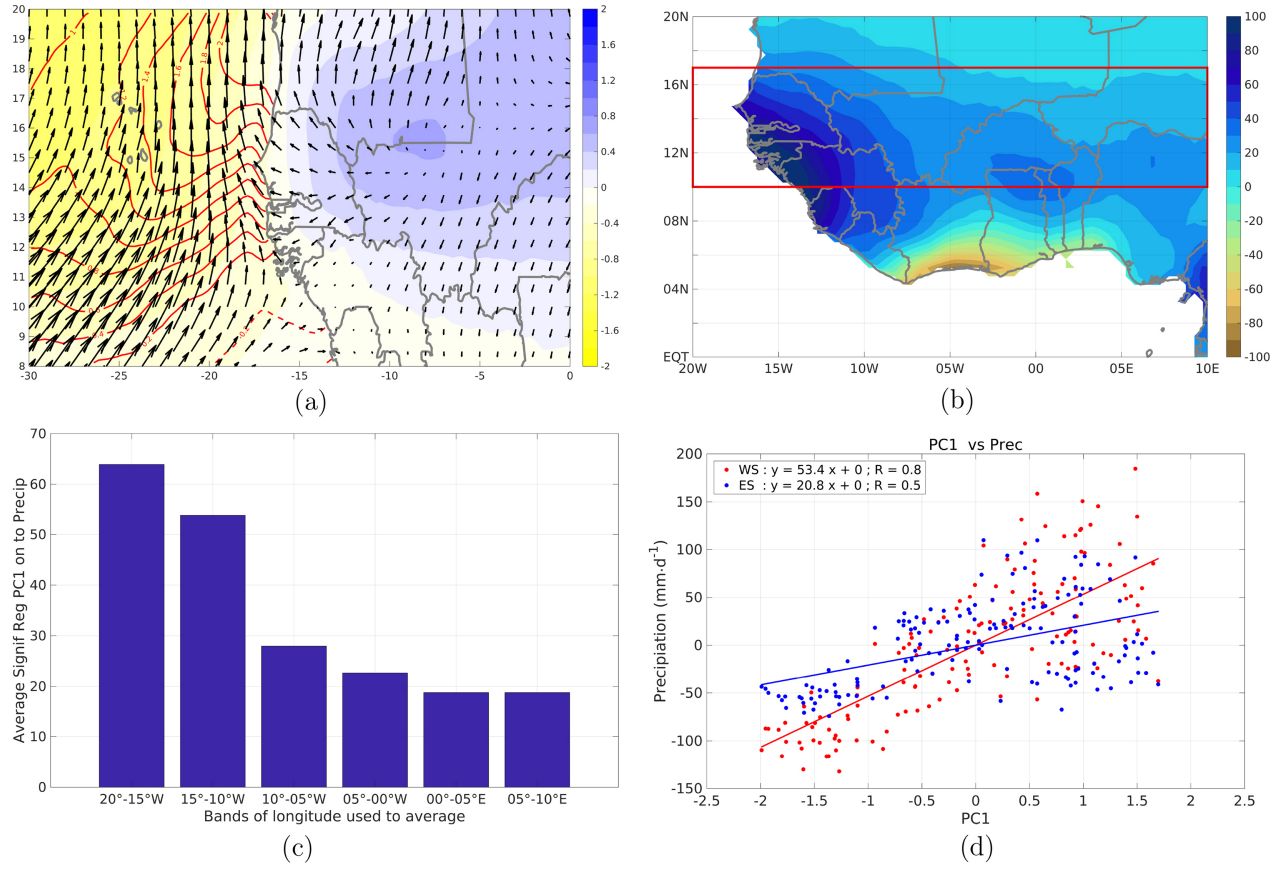

Figure 3. (a) Summer (June-September, JJAS) mean sea level pressure (shading: Pa), 10-meter wind (vector: m·s^{-1} obtained by regressing against PC1 during 1982-2019 and the associated SST anomalies pattern (red contours: ˚C). (b) JJAS mean precipitation (shading: mm·d^{-1}) 925 hPa wind (vector: m·s^{-1} and surface pressure (contour: Pa) obtained by regressing against PC1 during 1982-2019. (c) Linear regression coefficients of the JJAS mean PC1 with precipitation average into the Sahalian band by 5˚ of longitude from 20˚W to 10˚E (red box). (d) scatter plot of JJAS mean precipitation average over the Western Sahel (WS: 20˚ - 10˚W, red dots) and Eastern Sahel (ES: 10˚W - 10˚E, bleu dots), the horizontal axis is the value of PC1. The red (blue) solid line denotes the linear regression for the WS (ES) region, and the regression equation and its associated correlation coefficients are shown on the top of the panel.

(red box in **Figure 3(b)**) per 5˚ of longitude from 20˚W to 10˚E. This figure shows the strongest regression coefficients (60 mm·d^{-1}·C^{-1}) value occurs in the west of 10˚W while the lowest ones (20 mm·d^{-1}·C^{-1}) is observed in the eastern region of 10˚W. This is in agreement with [14] in the Indian Ocean. They show that when a Ningaloo Niño develops, remarkably enhanced precipitation anomalies occur primarily off the coast of northwestern Australia (NWA) rather than over the offshore area of western Australia, where the most significant sea surface temperature warming prevails. This enhanced NWA precipitation manifests as jointly intensified stratiform and convective precipitation accompanied by an increase in high cloud cover. **Figure 3(d)** depicts the relationships between the NTA warm anomalies and the variation of precipitation over the western and eastern Sahelian regions (WS and ES, respectively). The area-averaged total precipitation anomalies show a significant positive correlation with the NTA warm anomalies over the WS region with a coefficient value of +0.8 while a weaker

value of +0.5 is observed over the ES region. In addition, the regression coefficient for the WS region is 2.5 times greater than the one for ES region, indicating that the WS precipitation is more sensitive to the intensity of the NTA warm events.

Figure 4 shows the behavior of West African rainfall, particularly in the Sahel, in response to warm and cold events in the NTA region. Figure 4(b) shows an increase in Sahelian rainfall (10˚ - 18˚N) associated with the warming of the NTA SST (Figure 4(a)). The composite of warm years shows the presence of very warm water located North of 17˚N and West of 20˚W with a maximum anomaly value of +0.8˚C (Figure 4(a)). The figure also highlights that the warm waters are almost present over the whole area and the coldest waters are located South of 12˚N with an anomaly of +0.15˚C. Thus this southward propagation of warm waters generates strong meridional SST gradients in the NTA that play an active role in forcing convection over the ocean by organizing convergence in the lower layers [42], a mechanism that can enhance rainfall over the continent. The surface wind pattern associated with the warm composite shows a strengthening of the northward circulation and a strong surface convergence anomaly in the WS region co-located with the strongest positive rainfall anomaly.

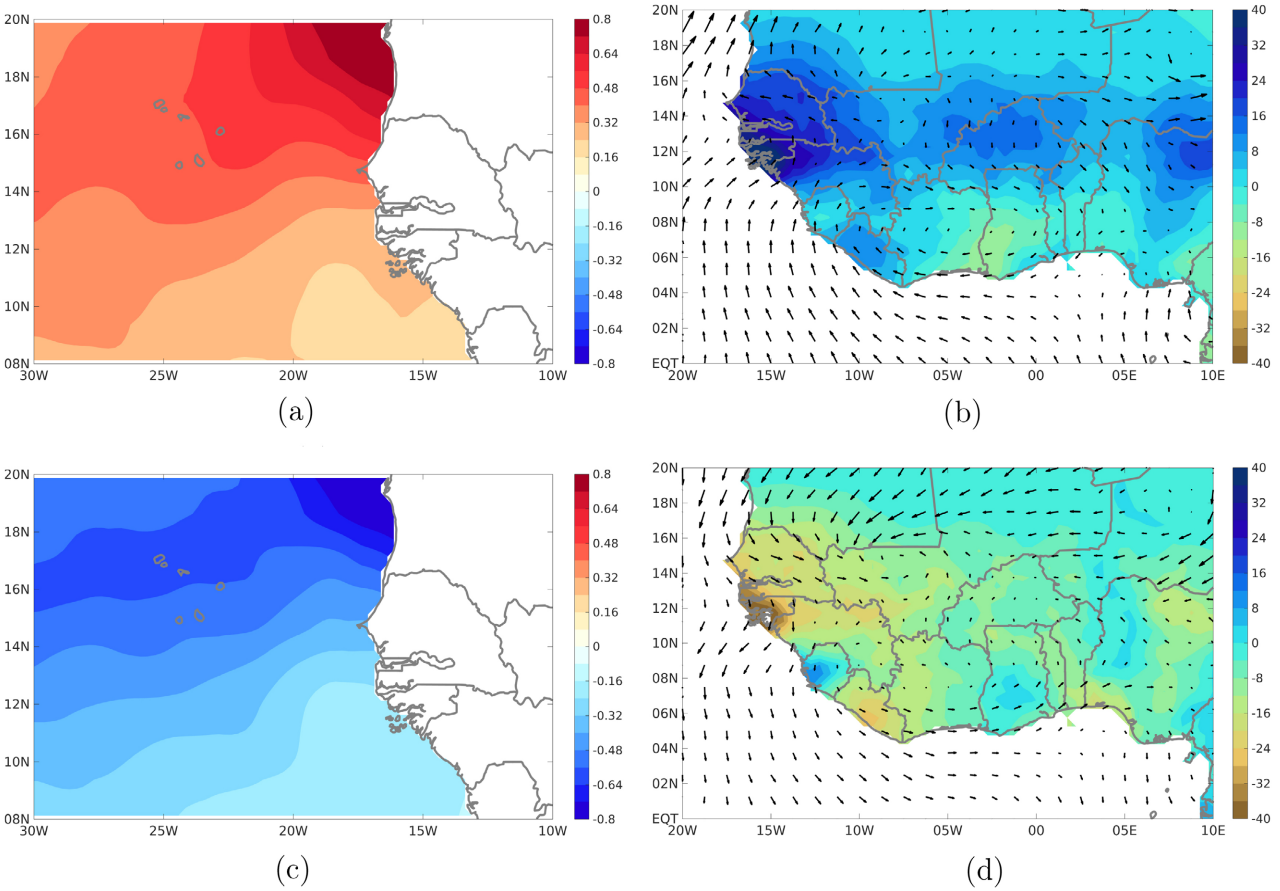

Figure 4. Warm ((a) and (b)) and cold ((c) and (d)) composites of SST (left column: ˚C) and precipitations (right column: mm·d^{-1}). For (b) and (d) are showing the 925 hPa horizontal wind (vector: m·s^{-1}) anomalies in June-September 1982-2019.

The opposite mechanism is observed during cold years of NTA (**Figure 4(c)** and **Figure 4(d)**). According to the Wind-Evaporation-SST (WES or Bjerknes) mechanisms, a cold SST anomaly induces a southward acceleration of the northern wind (**Figure 4(d)**) and thus limits the penetration of the convergence zone to the north during this period (June-September). This results in a southern location of the rain zone with regard to its climatological mean position and therefore with less precipitation over the regions of interest. This is confirmed by studies of the relationship between ACT and ITCZ (or WAM) northward migration ([7] [42] [43]). They show that a northward acceleration of the southerly wind results from cold SST anomalies in the ACT region, leading to a northward migration of the ITCZ and associated West African rainfall. **Figure 4(d)** shows negative rainfall anomalies over West African regions, except for mountainous regions (*i.e.* Guinean regions). However, this decreasing trend in rainfall is more pronounced over the WS, particularly over Senegal and it can be explained by the low-level anomalous atmospheric circulation in this region (WS). On one hand, the surface wind composite shows a divergence, which is more pronounced over the north of Senegal (North of 16˚N). On the other hand, the low-level circulation anomaly shows weak oceanic flow penetrating the continent that induces weak moisture transport into the continent.

According to [44], the precipitation variability is strongly correlated with that of precipitable water, showing the existence of a threshold relationship between these variables. This relationship results in a band of heavy precipitation located above areas of high PWV (larger than 50 $kg \cdot m^{-2}$), suggesting that little (or no) precipitation is observed over areas of PWV less than 50 $kg \cdot m^{-2}$. However, PWV is controlled by moisture flux, *i.e.* moisture transport [34], showing the importance of understanding the distribution of precipitable water. Thus, **Figure 5** shows the composites of precipitable water anomalies associated with the NTA warm and cold events. The composite analysis shows a positive (negative) precipitable water anomaly associated with the warming (cooling) of the SST in the NTA, reflecting a moistening (drying) of the atmospheric column.

A warm event in the NTA region induces moisture transport further north in the Sahelian region (north of 12˚N), with more pronounced transport from the ocean to the continent in the lower layers (from surface to 850 hPa, **Figure 5(a)**). This figure shows that the highest amount of precipitable water in the lower layers is located north of 12˚N, especially in the western region of 10˚W. However, all this moisture is transported to higher altitudes by the ascending branch of the convergence zone (**Figure 4(b)**) and, there is humidification of the atmospheric middle layers (700 - 500 hPa, **Figure 5(c)**). The deceleration of the upper jets (*i.e.* AEJ), at this level, leads to a weakening of the transport of moisture available for rain towards the west. Whereas at high altitudes (400 - 100 hPa, **Figure 5(e)**), the divergent circulation of the upper air jets (*i.e.* TEJ) transports all the moisture to the west. This pattern of moist air mass circulation associated with a deep convection zone is favorable for precipitation.

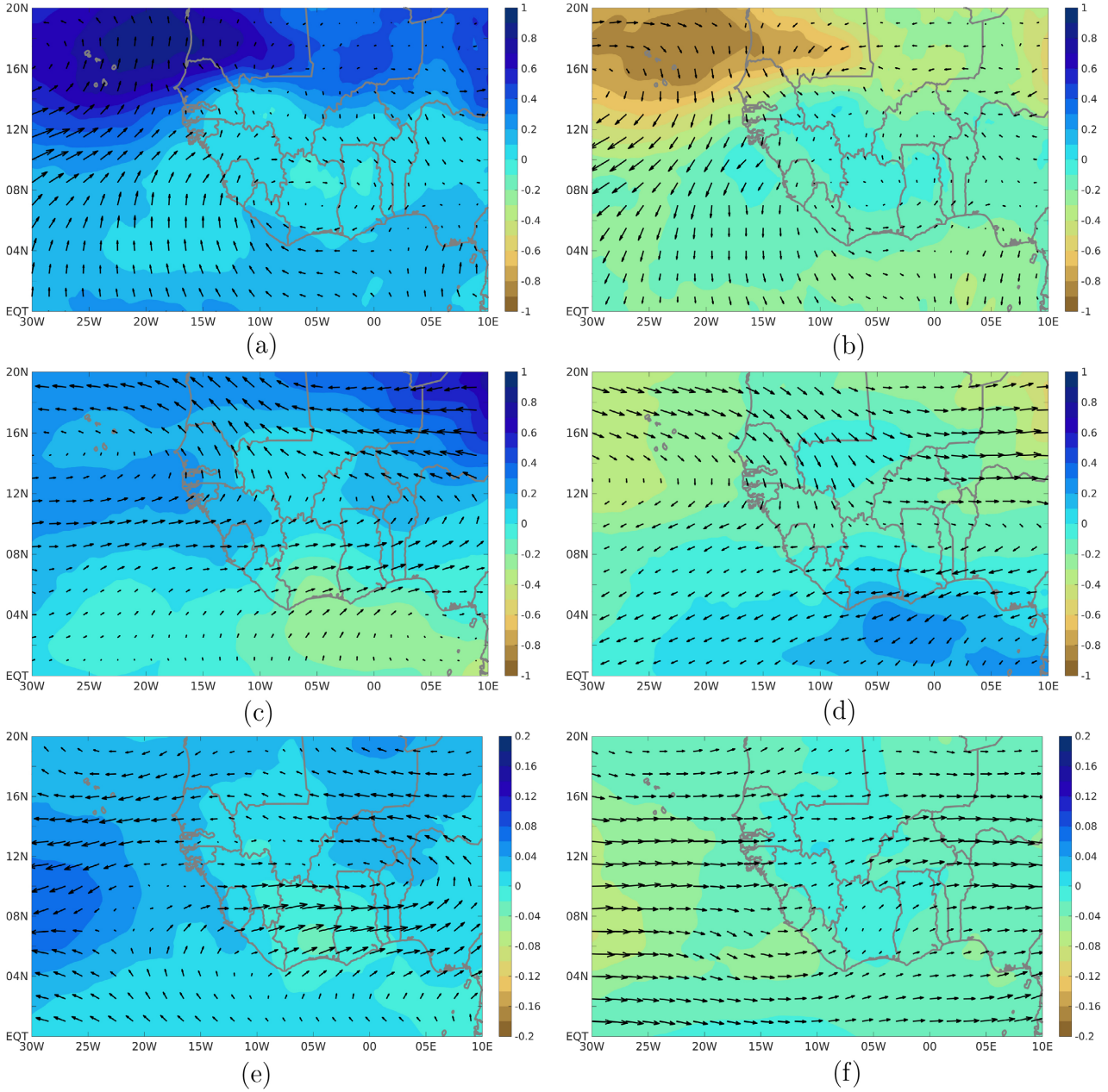

Figure 5. Same in **Figure 4** but for precipitable water vapor (PWV, shading) and moisture transport (vector): ((a) WARM 1000 - 850 hPa and (b) COLD 1000 - 850 hPa) in the lower layers (from the surface pressure, P_{surf} to 850 hPa), ((c) WARM 700 - 500 hPa and (d) COLD 700 - 500 hPa) middle layers (700 - 500 hPa), and ((e) WARM 400 - 100 hPa and (f) COLD 400 - 100 hPa) upper layers (400 - 100 hPa). Left column (composite warm) and right column (composite cold).

On the other hand, during a cold event in the NTA region, there is a considerable reduction of precipitable water in the lower layers (**Figure 5(b)**) north of 12˚N in the western region of 10˚W associated with a strong southward moisture transport, thus creating divergence of the moisture flow in this region. This drying of the air masses in the lower layers could induce shallow lift (weak convection) in this region. In the middle layers (**Figure 5(d)**), a negative precipitable water anomaly is also noted associated with the strengthening of the upper

jets (divergent circulation) at this level. In the upper layers, a reduction in the moisture transport by the upper jets (**Figure 5(f)**) can be observed throughout the study region. In contrast to the warm composite, this air mass circulation is typical of shallow (or dry) convection and is unfavorable for increasing precipitation in the region.

3.2. Large Scale Atmospheric Circulation Anomalies Associated with the NTA Warm/Cold

This section depicts the large-scale atmospheric circulation anomalies associated with the warming and cooling NTA region.

In the atmospheric lower layer, the warming of the NTA SST induces a cyclonic circulation around the low-pressure anomaly and considerably reduces the intensity of the northerly winds (**Figure 6(a)**). This results in a convergence of surface winds in the region of the oceanic ITCZ. Over West Africa, a divergence/convergence dipole centered on 13˚N is observed in association with the surface wind circulation (**Figure 6(a)**). Indeed, the cooling of the NTA SST, favoring an anticyclonic circulation resulting from the high pressure, leads to an acceleration of the northerly winds, thus creating a divergence of the surface wind (**Figure 6(b)**). As opposed to the warm composite, the circulation of the lower layer winds associated with the cooling of the SST induces an opposite dipole with convergence to the north of 13˚N (**Figure 6(b)**). In the middle layers (500 hPa), the most dominant signal of the atmospheric circulation is the significant reduction (acceleration) of the upper jets, particularly the African Easterly Jet (AEJ), in response to the warming (cooling) of the SST (**Figure 6(c)** and **Figure 6(d)**), respectively. While in the upper troposphere, we observe a strengthening of the tropical easterly jets (TEJ) for the warm composite (**Figure 6(e)**), contrary to the cold composite which contributes to the weakening of the easterly winds (**Figure 6(f)**). In the upper troposphere, the dominant signal for circulation is the divergence (convergence) of the winds associated with the warming (cooling) of the NTA SST. Except in the western 10˚W region between 8˚N and 14˚N where there is a convergence (divergence) of surface winds. The spatial distribution of the relative humidity anomaly associated with the warm and cold composites is strongly correlated with that of the atmospheric circulation for each composite. Indeed, the atmospheric circulation shows a northward (southward) advection of moisture during a warm (cold) NTA event (**Figure 7(a)** and **Figure 7(b)**). During a warm (cold) SST event, the highest (lowest) moisture amount is located towards the coast north of 14˚N over the ocean. In contrast, over West Africa, the warming (cooling) of the SST leads to a positive (negative) moisture anomaly north of 12˚N in association with the atmospheric circulation shown in **Figure 6(a)** and **Figure 6(b)**. In the Sahel, a considerable decrease in the amount of moisture increases (decrease) towards the east (**Figure 7(a)** and **Figure 7(b)**). For the warm composite, the co-location of the moisture accumulation zone (**Figure 7(a)**) and the divergence zone (**Figure 6(a)**) induces a high-latitude advection of moist air masses. As the warm and moist air particles

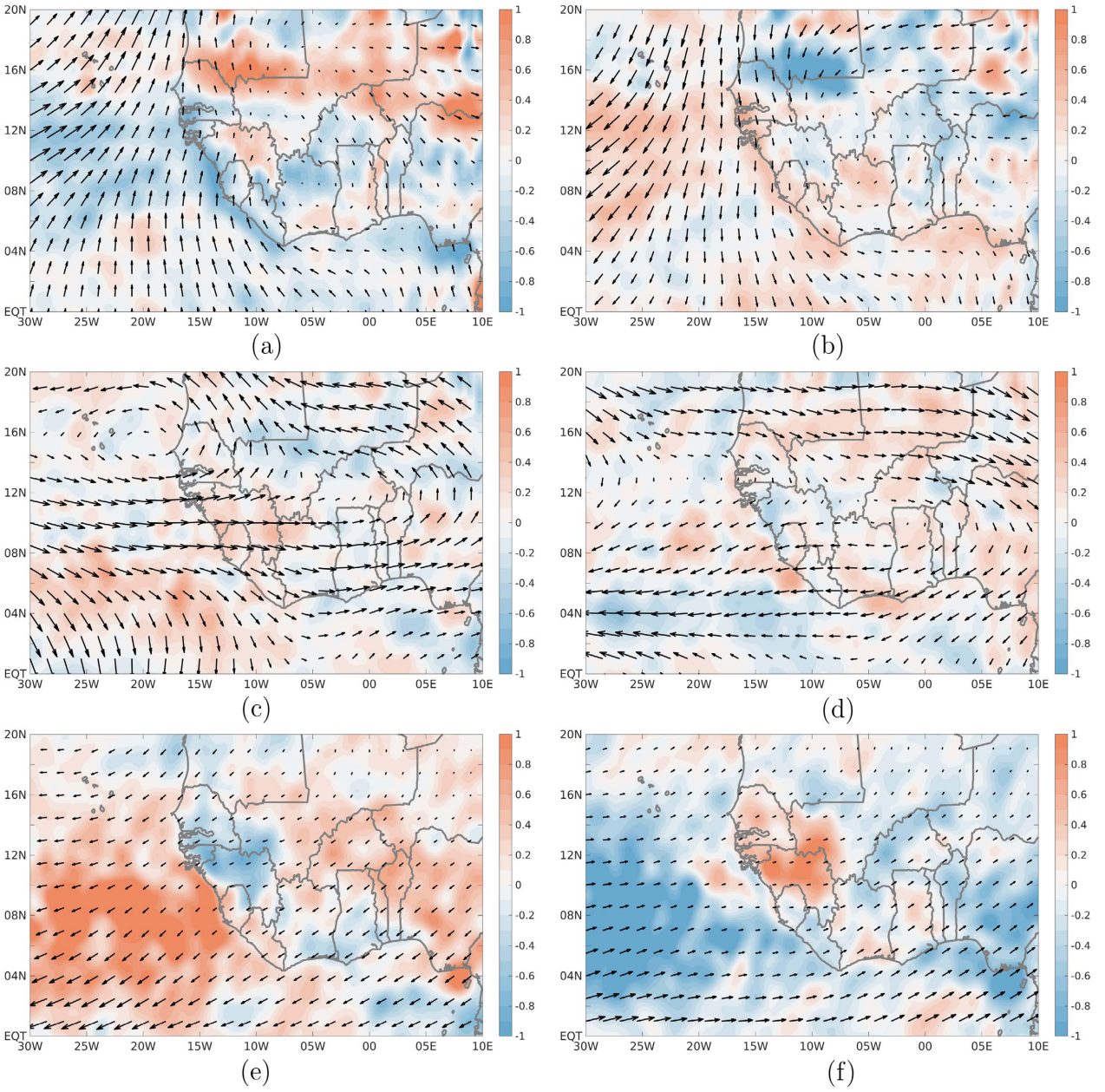

Figure 6. Same in **Figure 5** but for wind divergence ($\times 10^{-6}$ s^{-1} shading) and horizontal wind (vector) at 925 hPa ((a) WARM 925 hPa and (b) COLD 925 hPa), 500 hPa ((c) WARM 500 hPa and (d) COLD 500 hPa) and 200 hPa ((e) WARM 200 hPa and (f) COLD 200 hPa). Left column (composite warm) and right column (composite cold).

in the lower layers become colder and less moist, this leads to weak humidification of the upper layers (**Figure 7(c)**). The opposite is observed during the NTA cold event, where the atmospheric column dries out (**Figure 7(b)** and **Figure 7(d)**) due to atmospheric circulation. In summary, the atmospheric circulation and humidity distribution associated with the warm NTA events, which results in convergence in the lower layers and divergence at high altitudes, is favorable for an increase in rainfall. On the other hand, the cold composite induces an opposite effect and favors a reduction in precipitation. Indeed, the relationship

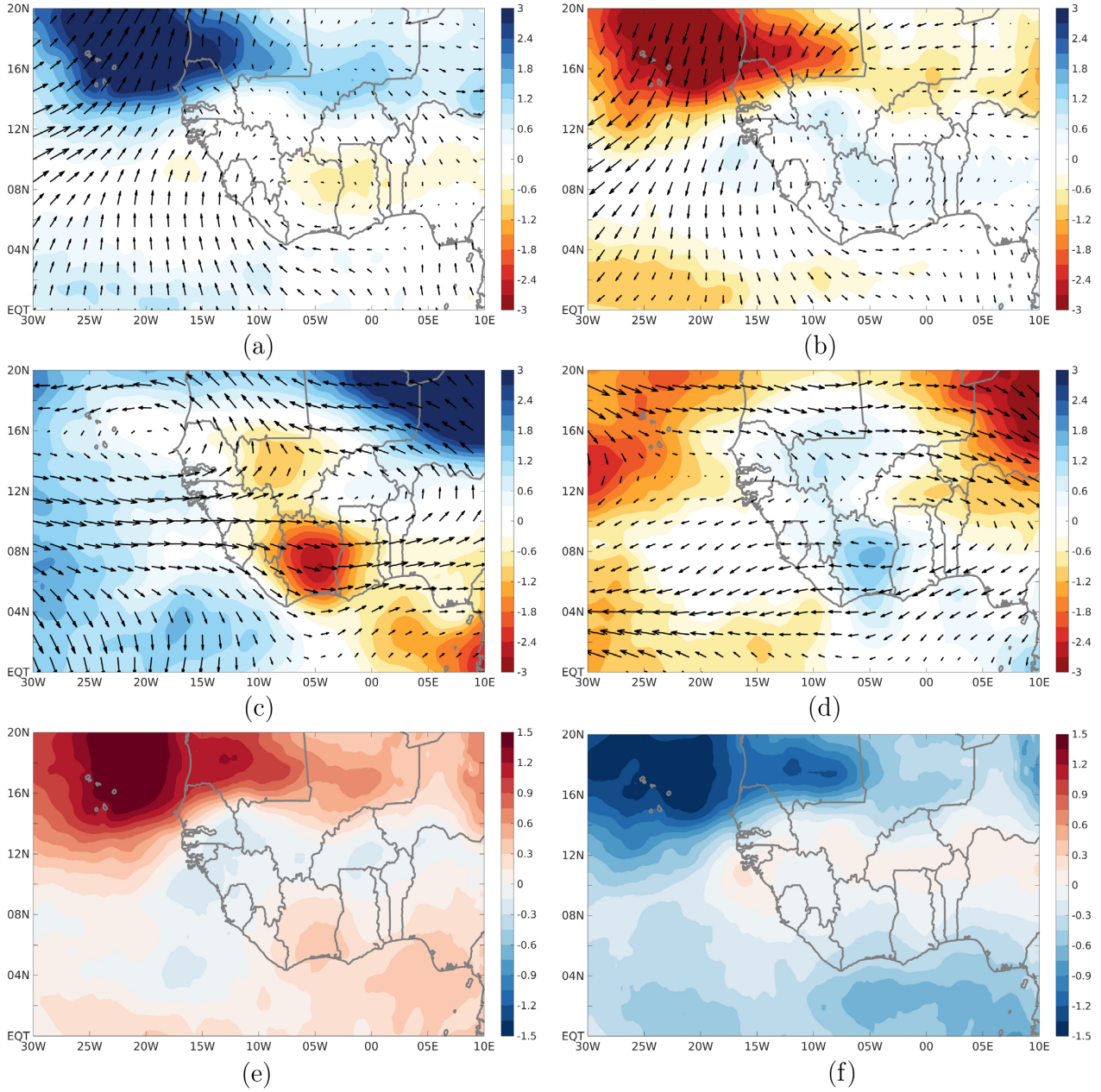

Figure 7. Same in **Figure 5** but for Relative humidity (shading) and horizontal wind (vector) at 925 hPa ((a) RH-WARM 925 hPa and (b) RH-COLD 925 hPa) and 500 hPa ((c) RH-WARM 500 hPa and (d) RH-COLD 500 hPa), and ((e) PC-WARM and (f) PC-COLD) are for the potential of convection (shading). Left column (composite warm) and right column (composite cold).

between atmospheric convection over West Africa and upper jets (AEJ, TEJ, and the sub-tropical westerly jet (STWJ)) is clearly shown in previous studies in association with African Easterly waves, AEW, ([45] [46] [47] [48]). [45] shows that the anomalies in the large-scale circulation also change the vertical wind shear and the strength, position, and instability of the African easterly jet, which in turn leads to changes in interannual African easterly wave activity and Sahel rainfall. The AEJ is a key feature of the West African monsoon (WAM), linking large-scale aspects of the WAM to its characteristic weather systems [49]. Its

vertical shear is important for the growth of long-lived mesoscale convective systems (MCSs) [50] and its potential vorticity (PV) and low-level temperature contrasts are important for African-easterly-wave (AEW) development [51]. In [52] the WAM system is characterized by a strong JET at 200 hPa and an AEJ less intense than the first generating moist and deep convection in the ITCZ to the south of the ITD. This is confirmed by cloud-resolving model (CRM) simulations and idealized models ([53] [54]) who show associated the activation of the convection to upper-level anticyclonic and divergent flow feeds the tropical easterly jet (TEJ) and subtropical jet (STJ) on their southern and northern flank, leading to fast displacement of the mesoscale convective systems (MCSs, [55]) account for most of the rain over the Sahel.

After diagnosing the difference between the impacts of the two composites of SST on the atmospheric circulation using dynamical parameters, the mean state of the atmosphere is assessed using thermodynamic parameters such as the Potential of convection (Pc, **Figure 7(e)** and **Figure 7(f)**). Following [56], Pc is the difference between the equivalent potential temperature at 1000 hPa (surface) and 500 hPa (mid-troposphere):

$$\mathrm{Pc} = \theta_e(1000) - \theta_e(500), \tag{3}$$

where θ_e is the equivalent potential temperature. The potential of convection is a good parameter for studying the degree of atmospheric instability. High values of Pc (≥14 K) are necessary for the development of deep convection. Over West Africa, a dipole of Pc anomalies is observed with a strengthening of the convection north of 13˚N and a weakening in the south associated with warming in the NTA region (**Figure 7(e)**). The opposite dipole is noted during the cooling of the SST in the NTA (**Figure 7(f)**). Furthermore, a zonal gradient of the Pc anomaly is noted with the highest values found in the west and a progressive attenuation of the anomaly intensity towards the east in the Sahel (**Figure 7(e)** and **Figure 7(f)**). This shows a strengthening (weakening) of the convective activity in the Sahel with the largest contribution in the western Sahel (WS), in association with the warming (cooling) SST events. This may partly explain the increased or decreased rainfall in the Sahel region associated with NTA warm or cold events, respectively. Note also the high degree of correlation between the spatial distribution of relative humidity anomalies and convective potential. This result is consistent with [56] who show that the difference in Pc between AEWs associated with and without cyclones shows an axis of maximum positive values along 15˚N, which extends well into the North Atlantic Ocean, indicating that the atmosphere is more unstable for the cases of AEWs associated with cyclones. This northward shift in the peak in Pc for AEWs with cyclones corresponds to a general northward shift in the monsoon trough. [56] show that this greater instability is associated with the presence of a monsoon layer deeper in latitude and more intense in magnitude.

The complete analysis of the effect of the SST anomaly in the NTA region on the atmospheric circulation is shown in **Figure 8**, averaged over the western

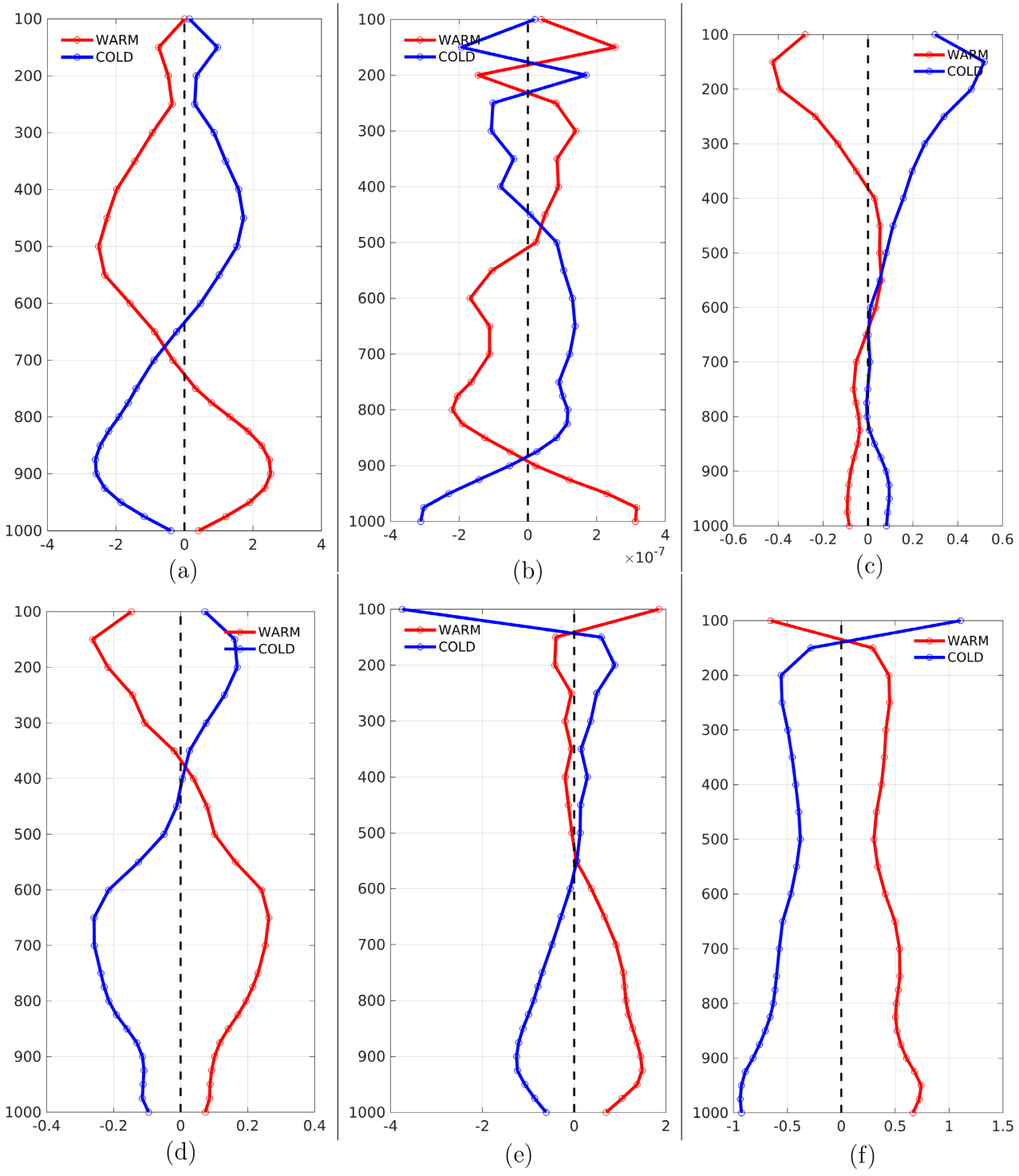

Figure 8. Same in **Figure 5** but average over the western Sahel (WS) region for (a) Vertical velocity (Omega × 10^{-3}, Pa·s^{-1}), (b) Wind divergence × 10^{-7} (s^{-1}), (c) Zonal wind (m·s^{-1}), (d) Meridional wind (m·s^{-1}), (e) Relative humidity (%) and (f) Potential temperature (K). The red (blue) curve is shown the composite warm (cold) during 1982-2019.

Sahelian region, particularly Senegal. Overall, the warming and cooling of the NTA SST induce opposite effects on the atmospheric circulation in the whole troposphere. During an NTA warm event, the tropospheric column is marked by

an acceleration of the vertical velocity in the lower layers with a maximum velocity recorded around 925 hPa (**Figure 8(a)**). In the upper layers, there is a progressive decrease of the vertical velocity until 500 hPa. This vertical velocity structure induced by the NTA SST anomalies correlates well with that of the divergence (**Figure 8(b)**). This figure shows the convergence/divergence inversion at the maximum vertical velocity anomaly altitudes (**Figure 8(a)**). Indeed, the lower and upper layers are governed by divergence which is more important in the lower troposphere, while the middle layer is dominated by wind convergence (**Figure 8(b)**). **Figure 8(c)** shows that the NTA SST anomaly has a weak influence on the vertical structure of the zonal wind in the lower and middle layers, while in the upper troposphere, the warming is associated with an acceleration of the easterly jets with a maximum observed around 200 hPa. For the meridional wind (**Figure 8(d)**), the warming of the SST induces a strengthening of the southerly wind from the surface up to 350 hPa with a maximum wind acceleration noted in the lower layer around 650 hPa. From 350 hPa, there is a progressive slowing down of the meridional wind. Thus, this atmospheric circulation, associated with the warm and cold composites of NTA, largely explains the vertical distribution of relative humidity (**Figure 8(e)**) and potential temperature (**Figure 8(f)**) of air masses in the troposphere. **Figure 8(e)** shows that in the WS (or Senegal) region, a warm NTA SST event is associated with an anomalously moist layer, from the surface to 550 hPa, with a moisture maximum recorded around 925 hPa. From 550 hPa, there is a very small decrease in relative humidity. Thus, we speak of deep and humid atmospheric convection. This deep and moist convection over the WS region is also explained by the thermal instability of the atmospheric column. **Figure 8(f)** shows a gradual cooling of the air mass temperature throughout the troposphere during an NTA warm event. The instability is marked by the presence of lighter (warmer and wetter) air masses in the lower layers and heavier (colder and less wet) air masses in the upper layers (**Figure 8(e)** and **Figure 8(f)**). Indeed, the instability is more important between 925 hPa and 500 hPa where the air cools down very quickly, while from 500 hPa there is a small increase in air temperature (**Figure 8(f)**). In summary, this shows that a warming of the SST in the NTA region enhances the atmospheric conditions favorable for increased rainfall in the WS region, particularly Senegal. The opposite is observed during periods of SST cooling, where conditions tend to stabilize the atmospheric column and thus reduce rainfall in this region (**Figure 8**).

In summary, this is in agreement with the results found that warming of the SST is one of the actors contributing to the increase in Sahelian rainfall, particularly in the western region (or Senegal). On the other hand, an abnormally cold NTA event contributes to the decrease in rainfall in the Sahel, with a considerable reduction towards the coast.

4. Conclusions

In this study, we investigated the influence of the northeastern tropical Atlantic

(NTA) on the West African rainfall, particularly in the Sahel, as well as the associated dynamic mechanisms on the inter-annual times scale. The empirical orthogonal function (EOF) shows that the dominant mode of the SST variability (87.4%) is characterized by a warming SST off the West African coast. The principal component (PC1) associated with this EOF is well correlated (+0.97) with the NTA index (NTAI) defined as the averaged SST anomalies (SSTA) in the region of 12˚ - 16˚N of the East of 25˚W.

The linear regression of PC1/NTAI of the West African rainfall and atmospheric variables shows that the influence of the NTA index (NTAI) on West African rainfall is stronger in the western regions (West of 10˚W) and decreases considerably towards the east. Over the Sahel, the regression coefficients allowed us to show that the impact of the NTAI is three times greater in the west of 10˚W than in the eastern part, indicating that the western Sahel (west of 10˚W, WS) rainfall is more sensitive to the NTA SST anomalies.

The surface wind pattern associated with the warm composite shows a strengthening of the northward circulation and a strong surface convergence anomaly in the WS region co-located with the strongest positive rainfall anomaly. The opposite mechanism is observed with cold composite where a cold SST anomaly induces a southward acceleration of the northern wind and thus limits the penetration of the convergence zone to the north during this period (June-September). Then, warming (cooling) events in this Atlantic region contribute to an increasing (decreasing) of rainfall in the Sahel with a maximum noted in the western regions, particularly over Senegal.

In the atmospheric lower layers, the warming of the NTA SST induces a cyclonic circulation around the low-pressure anomaly and considerably reduces the intensity of the northerly winds. While the cooling event favors an anticyclonic circulation resulting from the high pressure, leading to an acceleration of the northerly winds. The atmospheric circulation response, to the warming (cooling) NTA, in the middle layer (500 hPa) dominates a significant reduction (acceleration) of the upper-level jets (African Easterly Jet, AEJ). While in the upper troposphere, we observe a strengthening of the tropical easterly jets (TEJ) for the warm composite, contrary to the cold SST composite which contributes to the weakening of the easterly winds.

In terms of humidity transport (or advection), the warming event induces a northward moisture transport in the Sahel region (north of 12˚N), with more pronounced transport from the ocean to the continent in the lower layers (from surface to 850 hPa) leading to a high amount of precipitable water to the north of 12˚N, especially in the western region. During the cold event in the NTA region, we have the opposite mechanism resulting in strong southward moisture transport. Then, the cold composite is associated with less precipitable water vapor and a weakening of convection leading to a decrease of the precipitation over Sahel.

Figure 9 shows a strong relationship between the NTA and rainfall index over the Sahel (9a), which is more significant over Senegal (9b) on a decadal scale. It

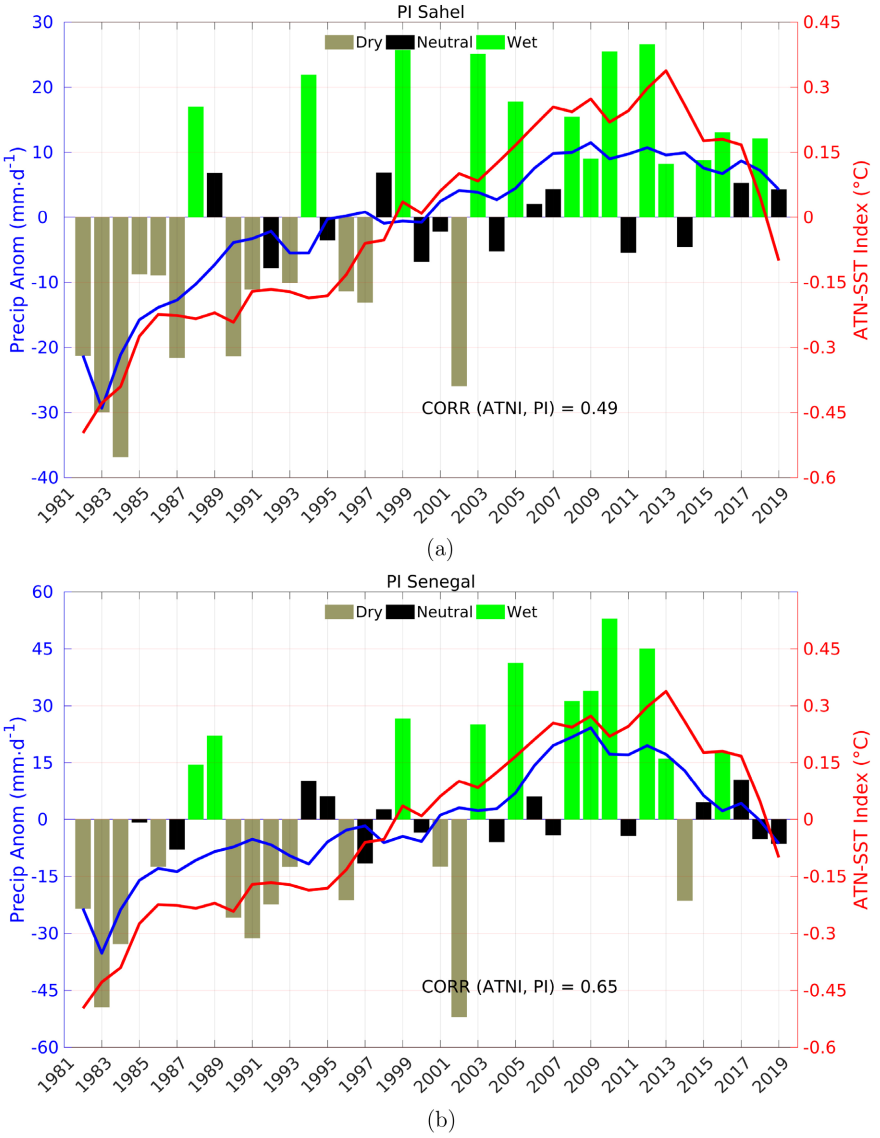

Figure 9. Bar plots of precipitation anomalies index over Sahel (20˚W - 10˚E, 12˚ - 18˚N) (a) and Senegal (18˚ - 11˚W, 12˚ - 17˚N) (b). The red (blue) curve shows the time series of the precipitation (NTAI) anomalies smoothed over 10 years and their correlation coefficient is shown below for each panel.

shows the important role of NTA SST anomalies on Sahelian rainfall. However, our results show that this influence is more significant in the western Sahel region (Senegal). Hence the interest to consider this SST anomaly index in weather forecasts in the Sahel, particularly in Senegal.

Acknowledgements

We thank the anonymous reviewers for their comments on the manuscript. The reanalyses ERA5 data sets are provided by the European Center for Medium-Range Weather Forecasts (ECMWF, https://cds.climate.copernicus.eu/), the precipitation data are from the Climatic Research Unit gridded Time Series (CRU-

TS4.04, https://data.ceda.ac.uk/) and the sea surface temperature data are obtained from the National Oceanic and Atmospheric Administration (NOAA) Optimal Interpolated Sea Surface Temperature (OISST, https://psl.noaa.gov/data/gridded/). This work was supported by UK Research and Innovation as part of the Global Challenges Research Fund, grant number NE/P021077/1 (GCRF African SWIFT) and Ecole Supéreure Polytechnique (https://esp.sn/) of the Cheikh Anta Diop University.

Conflicts of Interest

The authors declare no conflicts of interest regarding the publication of this paper.

References

[1] Oettli, P., Morioka, Y. and Yamagata, T. (2016) A Regional Climate Mode Discovered in the North Atlantic: Dakar Niño/Niña. *Scientific Reports*, **6**, Article No. 18782. https://doi.org/10.1038/srep18782

[2] Feng, M., McPhaden, M., Xie, S.-P. and Hafner, J. (2013) *La Niña* Forces Unprecedented Leeuwin Current Warming in 2011. *Scientific Reports*, **3**, Article No. 1277. https://doi.org/10.1038/srep01277

[3] Kataoka, T., Tozuka, T., Behera, S. and Yamagata, T. (2014) On the Ningaloo Niño/Niña. *Climate Dynamics*, **43**, 1463-1482. https://doi.org/10.1007/s00382-013-1961-z

[4] Zhang, L., Han, W., Li, Y. and Shinoda, T. (2018) Mechanisms for Generation and Development of the Ningaloo Niño. *Journal of Climate*, **31**, 9239-9259. https://doi.org/10.1175/JCLI-D-18-0175.1

[5] Doi, T., Tozuka, T. and Yamagata, T. (2010) The Atlantic Meridional Mode and Its Coupled Variability with the Guinea Dome. *Journal of Climate*, **23**, 455-475. https://doi.org/10.1175/2009JCLI3198.1

[6] Amaya, D.J., DeFlorio, M.J., Miller, A.J. and Xie, S.-P. (2017) WES Feedback and the Atlantic Meridional Mode: Observations and CMIP5 Comparisons. *Climate Dynamics*, **49**, 1665-1679. https://doi.org/10.1007/s00382-016-3411-1

[7] de Coëtlogon, G., Janicot, S. and Lazar, A. (2010) Intraseasonal Variability of the Ocean—Atmosphere Coupling in the Gulf of Guinea during Boreal Spring and Summer. *Quarterly Journal of the Royal Meteorological Society*, **136**, 426-441. https://doi.org/10.1002/qj.554

[8] Tian, B. and Ren, H.-L. (2022) Diagnosing SST Error Growth during ENSO Developing Phase in the BCC_CSM1.1(m) Prediction System. *Advances in Atmospheric Sciences*, **39**, 427-442. https://doi.org/10.1007/s00376-021-1189-5

[9] Li, T. and Philander, S.G.H. (1997) On the Seasonal Cycle of the Equatorial Atlantic Ocean. *Journal of Climate*, **10**, 813-817. https://doi.org/10.1175/1520-0442(1997)010<0813:OTSCOT>2.0.CO;2

[10] Xie, S.-P. and Philander, S.G.H. (1994) A Coupled Ocean-Atmosphere Model of Relevance to the ITCZ in the Eastern Pacific. *Tellus A*: *Dynamic Meteorology and Oceanography*, **46**, 340-350. https://doi.org/10.1034/j.1600-0870.1994.t01-1-00001.x

[11] Kusunoki, H., Kido, S. and Tozuka, T. (2020) Contribution of Oceanic Wave Propagation from the Tropical Pacific to Asymmetry of the Ningaloo Niño/Niña. *Climate Dynamics*, **54**, 4865-4875. https://doi.org/10.1007/s00382-020-05268-5

[12] Tanuma, N. and Tozuka, T. (2020) Influences of the Interdecadal Pacific Oscillation on the Locally Amplified Ningaloo Niño. *Geophysical Research Letters*, **47**, e2020GL088712. https://doi.org/10.1029/2020GL088712

[13] Xue, J., Luo, J.-J., Yuan, C. and Yamagata, T. (2020) Discovery of Chile Niño/Niña. *Geophysical Research Letters*, **47**, e2019GL086468. https://doi.org/10.1029/2019GL086468

[14] Zheng, T., Feng, T., Xu, K. and Cheng, X. (2020) Precipitation and the Associated Moist Static Energy Budget off Western Australia in Conjunction with Ningaloo Niño. *Frontiers in Earth Science*, **8**, Article 597915. https://doi.org/10.3389/feart.2020.597915

[15] Sultan, B. and Janicot, S. (2003) The West African Monsoon Dynamics. Part II: The "Preonset" and "Onset" of the Summer Monsoon. *Journal of Climate*, **16**, 3407-3427. https://doi.org/10.1175/1520-0442(2003)016<3407:TWAMDP>2.0.CO;2

[16] Okumura, Y. and Xie, S.-P. (2004) Interaction of the Atlantic Equatorial Cold Tongue and the African Monsoon. *Journal of Climate*, **17**, 3589-3602. https://doi.org/10.1175/1520-0442(2004)017<3589:IOTAEC>2.0.CO;2

[17] Biasutti, M., Battisti, D.S. and Sarachik, E.S. (2004) Mechanisms Controlling the Annual Cycle of Precipitation in the Tropical Atlantic Sector in an Atmospheric GCM. *Journal of Climate*, **17**, 4708-4723. https://doi.org/10.1175/JCLI-3235.1

[18] Giannini, A., Saravanan, R. and Chang, P. (2005) Dynamics of the Boreal Summer African Monsoon in the NSIPP1 Atmospheric Model. *Climate Dynamics*, **25**, 517-535. https://doi.org/10.1007/s00382-005-0056-x

[19] Meynadier, R., de Coëtlogon, G., Leduc-Leballeur, M., Eymard, L. and Janicot, S. (2016) Seasonal Influence of the Sea Surface Temperature on the Low Atmospheric Circulation and Precipitation in the Eastern Equatorial Atlantic. *Climate Dynamics*, **47**, 1127-1142. https://doi.org/10.1007/s00382-015-2892-7

[20] Tomaziello, A.C.N., Carvalho, L.M.V. and Gandu, A.W. (2016) Intraseasonal Variability of the Atlantic Intertropical Convergence Zone during Austral Summer and Winter. *Climate Dynamics*, **47**, 1717-1733. https://doi.org/10.1007/s00382-015-2929-y

[21] Crespo, L.R., Keenlyside, N. and Koseki, S. (2019) The Role of Sea Surface Temperature in the Atmospheric Seasonal Cycle of the Equatorial Atlantic. *Climate Dynamics*, **52**, 5927-5946. https://doi.org/10.1007/s00382-018-4489-4

[22] Nicholson, S.E. (2013) The West African Sahel: A Review of Recent Studies on the Rainfall Regime and Its Interannual Variability. *International Scholarly Research Notices*, **2013**, Article ID: 453521. https://doi.org/10.1155/2013/453521

[23] Diakhaté, M., Lazar, A., de Coëtlogon, G. and Gaye, A.T. (2018) Do SST Gradients Drive the Monthly Climatological Surface Wind Convergence over the Tropical Atlantic? *International Journal of Climatology*, **38**, e955-e965. https://doi.org/10.1002/joc.5422

[24] Brandt, P., Caniaux, G., Bourlès, B., Lazar, A., Dengler, M., Funk, A., Hormann, V., Giordani, H. and Marin, F. (2011) Equatorial Upper-Ocean Dynamics and Their Interaction with the West African Monsoon. *Atmospheric Science Letters*, **12**, 24-30. https://doi.org/10.1002/asl.287

[25] Liu, W., Cook, K.H. and Vizy, E.K. (2020) Role of the West African Westerly Jet in the Seasonal and Diurnal Cycles of Precipitation over West Africa. *Climate Dynamics*, **54**, 843-861. https://doi.org/10.1007/s00382-019-05035-1

[26] Pu, B. and Cook, K.H. (2012) Role of the West African Westerly Jet in Sahel Rainfall Variations. *Journal of Climate*, **25**, 2880-2896.

https://doi.org/10.1175/JCLI-D-11-00394.1

[27] Lélé, M.I. and Leslie, L.M. (2016) Intraseasonal Variability of Low-Level Moisture Transport over West Africa. *Climate Dynamics*, **47**, 3575-3591. https://doi.org/10.1007/s00382-016-3334-x

[28] Pu, B. and Cook, K.H. (2010) Dynamics of the West African Westerly Jet. *Journal of Climate*, **23**, 6263-6276. https://doi.org/10.1175/2010JCLI3648.1

[29] Hersbach, H., Bell, B., Berrisford, P., Hirahara, S., Horányi, A., Muñoz-Sabater, J., Nicolas, J., Peubey, C., Radu, R., Schepers, D., *et al.* (2020) The ERA5 Global Reanalysis. *Quarterly Journal of the Royal Meteorological Society*, **146**, 1999-2049.

[30] Reynolds, R.W., Smith, T.M., Liu, C., Chelton, D.B., Casey, K.S. and Schlax, M.G. (2007) Daily High-Resolution-Blended Analyses for Sea Surface Temperature. *Journal of Climate*, **20**, 5473-5496. https://doi.org/10.1175/2007JCLI1824.1

[31] Harris, I., Osborn, T.J., Jones, P. and Lister, D. (2020) Version 4 of the CRU TS Monthly High-Resolution Gridded Multivariate Climate Dataset. *Scientific Data*, **7**, Article No. 109. https://doi.org/10.1038/s41597-020-0453-3

[32] Cadet, D.L. and Nnoli, N.O. (1987) Water Vapour Transport over Africa and the Atlantic Ocean during Summer 1979. *Quarterly Journal of the Royal Meteorological Society*, **113**, 581-602. https://doi.org/10.1002/qj.49711347609

[33] Fontaine, B., Roucou, P., and Trzaska, S. (2003) Atmospheric Water Cycle and Moisture Fluxes in the West African Monsoon: Mean Annual Cycles and Relationship Using NCEP/NCAR Reanalysis. *Geophysical Research Letters*, **30**, Article No. 1117. https://doi.org/10.1029/2002GL015834

[34] Meynadier, R., de Coëtlogon, G., Bastin, S., Eymard, L. and Janicot, S. (2015) Sensitivity Testing of WRF Parameterizations on Air-Sea Interaction and Its Impact on Water Cycle in the Gulf of Guinea. *Quarterly Journal of the Royal Meteorological Society*, **141**, 1804-1820. https://doi.org/10.1002/qj.2483

[35] Bjerknes, J. (1969) Atmospheric Teleconnections from the Equatorial Pacific. *Monthly Weather Review*, **97**, 163-172. https://doi.org/10.1175/1520-0493(1969)097<0163:ATFTEP>2.3.CO;2

[36] Chang, P., Yamagata, T., Schopf, P., Behera, S.K., Carton, J., Kessler, W.S., Meyers, G., Qu, T., Schott, F., Shetye, S., *et al.* (2006) Climate Fluctuations of Tropical Coupled Systems—The Role of Ocean Dynamics. *Journal of Climate*, **19**, 5122-5174. https://doi.org/10.1175/JCLI3903.1

[37] Richter, I., Xie, SP., Morioka, Y., Doi, T., Taguchi, B. and Behera, S. (2017) Phase Locking of Equatorial Atlantic Variability through the Seasonal Migration of the ITCZ. *Climate Dynamics*, **48**, 3615-3629. https://doi.org/10.1007/s00382-016-3289-y

[38] Stevens, B., Duan, J., McWilliams, J.C., Münnich, M. and Neelin, J.D. (2002) Entrainment, Rayleigh Friction, and Boundary Layer Winds over the Tropical Pacific. *Journal of Climate*, **15**, 30-44. https://doi.org/10.1175/1520-0442(2002)015<0030:ERFABL>2.0.CO;2

[39] Lindzen, R.S. and Nigam, S. (1987) On the Role of Sea Surface Temperature Gradients in Forcing Low-Level Winds and Convergence in the Tropics. *Journal of Atmospheric Sciences*, **44**, 2418-2436. https://doi.org/10.1175/1520-0469(1987)044<2418:OTROSS>2.0.CO;2

[40] Sweet, W., Fett, R., Kerling, J. and La Violette, P. (1981) Air-Sea Interaction Effects in the Lower Troposphere across the North Wall of the Gulf Stream. *Monthly Weather Review*, **109**, 1042-1052. https://doi.org/10.1175/1520-0493(1981)109<1042:ASIEIT>2.0.CO;2

[41] Wallace, J.M., Mitchell, T.P. and Deser, C. (1989) The Influence of Sea-Surface Temperature on Surface Wind in the Eastern Equatorial Pacific: Seasonal and Interannual Variability. *Journal of Climate*, **2**, 1492-1499. 15https://doi.org/10.1175/1520-0442(1989)002<1492:TIOSST>2.0.CO;2

[42] Caniaux, G., Giordani, H., Redelsperger, J.-L., Guichard, F., Key, E., and Wade, M. (2011) Coupling between the Atlantic Cold Tongue and the West African Monsoon in Boreal Spring and Summer. *Journal of Geophysical Research*: *Oceans*, **116**, C04003. https://doi.org/10.1029/2010JC006570

[43] Foltz, G.R., Brandt, P., Richter, I., Rodríguez-Fonseca, B., Hernandez, F., Dengler, M., Rodrigues, R.R., Schmidt, J.O., Yu, L., Lefevre, N., Cotrim Da Cunha, L., McPhaden, M.J., Araujo, M., Karstensen, J., Hahn, J., Martín-Rey, M., Patricola, C.M., Poli, P., Zuidema, P., Hummels, R., Perez, R.C., Hatje, V., Lübbecke, J.F., Polo, I., Lumpkin, R., Bourlès, B., Asuquo, F.E., Lehodey, P., Conchon, A., Chang, P., Dandin, P., Schmid, C., Sutton, A., Giordani, H., Xue, Y., Illig, S., Losada, T., Grodsky, S.A., Gasparin, F., Lee, T., Mohino, E., Nobre, P., Wanninkhof, R., Keenlyside, N., Garcon, V., Sánchez-Gómez, E., Nnamchi, H.C., Drévillon, M., Storto, A., Remy, E., Lazar, A., Speich, S., Goes, M., Dorrington, T., Johns, W.E., Moum, J.N., Robinson, C., Perruche, C., de Souza, R.B., Gaye, A.T., López-Parages, J., Monerie, P.-A., Castellanos, P., Benson, N.U., Hounkonnou, M.N., Trotte Duhá, J., Laxenaire, R. and Reul, N. (2019) The Tropical Atlantic Observing System. *Frontiers in Marine Science*, **6**, Article 206. https://doi.org/10.3389/fmars.2019.00206

[44] Zhang, Y., Xu, J., Yang, N. and Lan, P. (2018) Variability and Trends in Global Precipitable Water Vapor Retrieved from Cosmic Radio Occultation and Radiosonde Observations. *Atmosphere*, **9**, Article No. 174. https://doi.org/10.3390/atmos9050174

[45] Thorncroft, C.D. and Rowell, D.P. (1998) Interannual Variability of African Wave Activity in a General Circulation Model. *International Journal of Climatology*, **18**, 1305-1323. https://doi.org/10.1002/(SICI)1097-0088(1998100)18:12<1305::AID-JOC281>3.0.CO;2-N

[46] Cornforth, R.J., Hoskins, B.J. and Thorncroft, C.D. (2009) The Impact of Moist Processes on the African Easterly Jet-African Easterly Wave System. *Quarterly Journal of the Royal Meteorological Society*, **135**, 894-913. https://doi.org/10.1002/qj.414

[47] Wang, Z. and Elsberry, R.L. (2010) Modulation of the African Easterly Jet by a Mesoscale Convective System. *Atmospheric Science Letters*, **11**, 169-174. https://doi.org/10.1002/asl.262

[48] Lafore, J.-P., Flamant, C., Guichard, F., Parker, D.J., Bouniol, D., Fink, A.H., Giraud, V., Gosset, M., Hall, N., Höller, H., Jones, S.C., Protat, A., Roca, R., Roux, F., Saïd, F. and Thorncroft, C. (2011) Progress in Understanding of Weather Systems in West Africa. *Atmospheric Science Letters*, **12**, 7-12. https://doi.org/10.1002/asl.335

[49] Parker, D.J., Thorncroft, C.D., Burton, R.R. and Diongue-Niang, A. (2005) Analysis of the African Easterly Jet, Using Aircraft Observations from the JET2000 Experiment. *Quarterly Journal of the Royal Meteorological Society*, **131**, 1461-1482. https://doi.org/10.1256/qj.03.189

[50] Houze Jr., R.A. and Betts, A.K. (1981) Convection in Gate. *Reviews of Geophysics*, **19**, 541-576. https://doi.org/10.1029/RG019i004p00541

[51] Thorncroft, C.D. and Hoskins, B.J. (1994) An Idealized Study of African Easterly Waves. I: A Linear View. *Quarterly Journal of the Royal Meteorological Society*,

120, 953-982. https://doi.org/10.1002/qj.49712051809

[52] Lafore, J.-P. (2007) La mousson africaine. *Atmosphériques*, **33**, 8-9.

[53] Diongue, A., Lafore, J.-P., Redelsperger, J.-L. and Roca, R. (2002) Numerical Study of a Sahelian Synoptic Weather System: Initiation and Mature Stages of Convection and Its Interactions with the Large-Scale Dynamics. *Quarterly Journal of the Royal Meteorological Society*, **128**, 1899-1927. https://doi.org/10.1256/003590002320603467

[54] Peyrillé, P. and Lafore, J.-P. (2007) An Idealized Two-Dimensional Framework to Study the West African Monsoon. Part II: Large-Scale Advection and the Diurnal Cycle. *Journal of the Atmospheric Sciences*, **64**, 2783-2803. https://doi.org/10.1175/JAS4052.1

[55] Mathon, V., Laurent, H. and Lebel, T. (2002) Mesoscale Convective System Rainfall in the Sahel. *Journal of Applied Meteorology*, **41**, 1081-1092. https://doi.org/10.1175/1520-0450(2002)041<1081:MCSRIT>2.0.CO;2

[56] Camara, M., Diedhiou, A. and Gaye, A. (2011) African Easterly Waves and Cyclonic Activity over the Eastern Atlantic: Composite and Case Studies. *International Journal of Geophysics*, **2011**, Article ID: 874292. https://doi.org/10.1155/2011/874292